

Nanostructured DLC coatings for self-assembly applications

Victor Manuel Freire Soler

Dr. Enric Bertran, Dr. Carles Corbella, grup FEMAN, IN2UB, Departament de Física Aplicada i Òptica, Universitat de Barcelona

Abstract— The special characteristics and singular properties of diamond-like carbon (DLC) thin films deposited by pulsed DC plasma enhanced chemical vapor deposition (PECVD), such as hardness and wear resistance, are suitable for self assembly applications as protective coating and as nanostructured surfaces. In this master thesis project, nanostructured DLC surfaces will be designed and characterized for self-assembly applications. Sub-micron patterns were lithographed on silicon through laser lithography while contact angle, nanotribometer, atomic force microscopy (AFM) and scanning electron microscopy (SEM) were used to characterize the surface. DLC properties on lithographed surfaces such as hydrophobicity and hardness were improved with the proper relative quantity of CHF_3 , resulting in very high contact angles and low friction coefficients. Self assembly properties were tested with silica nanoparticles which were prepared with a sol-gel solution.

Index Terms— 5. Nanostructured Materials: Characterization, Diamond-Like Carbon (DLC) Thin Films, Fluorinated Amorphous Carbon (a-C:F), Lithography, Plasma Enhanced Chemical Vapor Deposition (PECVD), Self assembly.

I. INTRODUCTION

THE main goal of this work is the design and fabrication of nano/micrometric structures by laser lithography directly on silicon wafers, which have been coated with a fluorinated thin film (diamond-like carbon, DLC). After that, a surface and tribological characterization has been done.

Carbon is a relatively abundant element in nature and it constitutes one of the basic elements for life. It is widely used in industry for materials manufacturing too. The fundamental feature of carbon is its unique capability for combining with other elements. Hydrocarbons are formed by the grouping of carbon and hydrogen atoms either in chains (polymers) or in rings (benzene). The addition of methyl radicals, nitrogen, oxygen and other new elements provides more complex molecules (acids, alcohols), whose accumulation leads to polymeric structures. The peculiar electronic configuration of carbon atoms, $1s^2 2s^2 2p^2$, and the small energy difference between their 2p and 2s orbitals, compared to the binding energy of the carbon bonds, allow the electrons to rearrange in s and p mixed orbitals that enhance the binding energy with other atoms. This process is called hybridization and produces three different types of orbitals: sp , sp^2 and sp^3 . Due to this

variety of possible bonding configurations, carbon has a number of allotropes: graphene (sheet of sp^2 bonded carbons: σ bonds plus delocalized π bonds), carbon nanotubes and fullerenes (graphene sheets rolled over themselves forming cylinders or spheres, respectively), graphite (Bernal stack of graphene sheets), diamond (network of sp^3 bonded carbons) and amorphous carbon (cross-linked and non-organized carbon matrix with a mixture of sp^2 and sp^3 bonds) [2, 11].

Hard amorphous carbon thin films can be deposited by a different number of deposition techniques. First deposited in 1971 by Aisenberg and Chabot with an ion beam, [Aisenberg and Chabot, 1971] it was soon after deposited by RF plasma enhanced CVD (PECVD) by Ojha and Holland [Ojha and Holland, 1977]. In 1990, Lifshitz et al. described the so called subplantation model by which a progressive densification of the film's sub-surface by penetration of energetic ions was produced, associated to the formation of metastable sp^3 sites [Lifshitz et al., 1990]. An energy of 100 eV was established as the optimum for high hardness a-C films, [Robertson, 1994] although more recently studies have revealed that lower ion energy can produce equally high sp^3 fractions [1, 19].

There are many kind of lithography techniques commonly used for this purpose: optical lithography, it involves exposing a photoresin to visible or UV light; e-beam, very similar but with electrons and improving the resolution; focused ion beam (FIB), scratching and booting directly the surface with charged ions; and laser, the chosen method because of the duration of the process.

Applications of DLC surfaces are many: magnetic storage technology (hard disks and read/write heads), automotive industry (coated parts with DLC have a great performance), injection molding, etc. [1]. One of the main advantages of DLC films is their biocompatibility and antithrombogenicity. Such properties make them candidates for a number of medical applications where wear resistant coatings, such as prosthesis, or simply biocompatible parts are required [1]. The surfaces of the implants are exposed to the interaction with the body cells and fluids and to potential corrosive medium. These effects can include cellular damage, infections, blood coagulation (potentially leading to thrombosis) and failure of the implants. Coating the implants with protective films, which can reduce corrosion and wear, may prevent or alleviate the problems

described above and extend the lifetime of implants to the benefit of the patients. DLC, which is characterized by chemical inertness, corrosion and wear resistance, appears to be an ideal material for such purposes and its use for protecting implants has been suggested already in the early 1990s. As a beginning of this work, silica sub-micron particles will be tested to determine if they form arrays following the carbon coated lithographed structure [3].

The introduction of alloying elements in amorphous carbon thin films has been used for a long time to improve specific properties of the films depending on the aimed application. Some of the most studied modifications include the reduction of internal compressive stress with N, Si or metal incorporation; the decrease of surface energy with F and some metals; the reduction of friction coefficient with F and Si-O, or the modification of the electrical properties. Metal-containing films are probably the most known modification for mechanical applications where hardness and friction are especially important. Metals like Ta, W and Nb reduce films' intrinsic compressive stress while wear resistance and hardness do not suffer an important reduction if the content is low. Also surface properties are modified with metal incorporation. Al, Fe, Ni, Nb and Ti, for example, reduce surface free energy (SFE) with water contact angle, while, on the other hand, W slightly increases SFE. In addition to metals, the incorporations of Si, O, N or F in a-C films have been investigated too. In this case, O and N increase SFE, while Si and F reduce it. Interestingly, addition of both Si and O can reduce the SFE more than only with Si [15]. Among these elements, fluorine incorporation exhibits the highest water contact angles (more than 100°) and lowest surface energies (about 20 mJ/m²) [1].

Colloidal particles are small objects with at least one characteristic dimension comprised between 1 nm and 1 μm, their range of sizes being defined by the importance of the Brownian motion. They include slurries, clays, sols and aerosols, foams, proteins, viruses, bacteria and cells. The most experimentally studied and used examples of colloidal particles are silica colloids and polymer latexes [9]. In the past decades, the formation of highly ordered structures of colloidal particles with sufficiently large domain sizes has attracted a wide research interest, also given the ample range of possible applications for this novel class of materials. Two-dimensional assemblies have been used as arrays of microlenses in imaging and as physical masks in microlithography (also called nanosphere lithography) [17]; three-dimensional assemblies, also called synthetic opals, have been used as precursors in producing high-strength ceramics, as templates for porous silica membranes and as diffractive elements in the fabrication of optical components and photonic bandgap (PBG) structures. Several self-organizing techniques have been devised to assemble high-quality arrays of monodispersed colloidal. The synthesis of colloids of highly uniform size and shape (monodisperse) is very important for the self-assembly of crystalline arrays of large sizes, since uniformity and order affect the electronic, optical, magnetic and electrokinetic

properties of the resulting aggregates [9]. Attachment of these silica particles will depend on roughness of the surface and its nanostructures.

II. EXPERIMENTAL

A. Deposition technique, PECVD

As we told above, hard amorphous carbon thin films can be deposited by different deposition techniques. RF PECVD is one of the most widely used deposition technique for DLC films as well as arc cathode and sputtering [1].

The basic steps in any CVD process have been summarised in the following list [1]:

- (a) Transport of the reactants from the gas inlets to the reaction zone.
- (b) Reactions in vapour phase that form the gas precursors of the film and by-products.
- (c) Transport of the reactants and their products from the gas phase to the substrate.
- (d) Adsorption of these species on the substrate surface.
- (e) Surface diffusion, chemical reactions and incorporation of these species on different growth sites.
- (f) Desorption of the volatile by-products of surface reactions.
- (g) Transport of the by-products away from the reaction zone.

PECVD is an evolution over CVD processes, in which a electrically activated set of gas-phase and surface reactions produce a solid product at a surface [Lieberman and Lichtenberg, 1994]. In PECVD, both types of reactions are controlled by the plasma properties, because electron impact dissociation of the feed gas is possible for the typical energies ($T_e = 2-3$ eV) of electrons in a low-pressure discharge. Film precursors are generated in the plasma bulk, as dissociated species, and then condense onto the substrate. Although deposition rate is not heavily substrate-temperature dependant [1], film properties such as composition, stress, morphology or crystalline structure generally do. Thus low temperatures (25°C) are typically used to deposit amorphous materials. The type of electrical signal used to excite the plasma determines its electronic and ionic characteristics, which in turn, influence film's properties. Moreover, it restricts the type of materials that can be deposited. For insulating films, if the film is intended to grow on the cathode, an alternating signal must be provided so that electrical charge-up in the film does not limit deposition process. Several signals of this kind can be used, each one producing different results: RF (radio-frequency), pulsed RF, pulsed DC or MW (microwaves). In RF plasmas, electrons, as opposed to ions, are able to follow the electric field due to their high mobility (the electronic plasma frequency is much higher than 13.56MHz). For this reason, in electropositive plasmas, the regions close to the electrodes end up developing a positive spatial charge (more ions than electrons). These spatial charge zones are called plasma sheath. In addition, in this region there is an electric field

pointing towards the electrode. The rest of the plasma volume is approximately at a constant positive voltage.

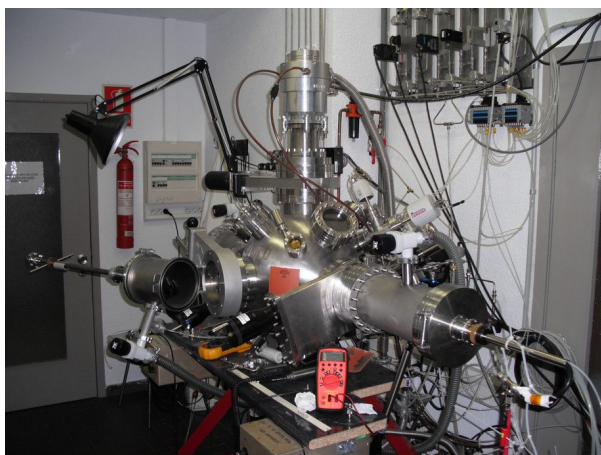
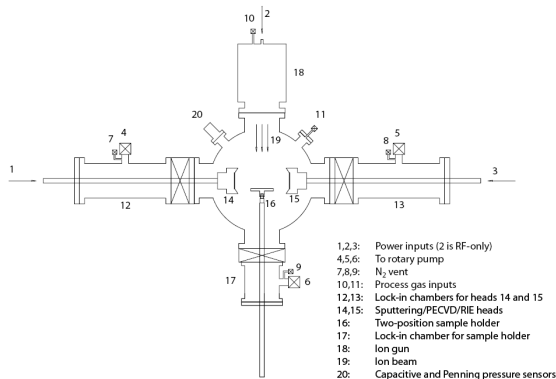


Fig. 1. Schematic figure of PEDRO (Plasma Etching and Deposition ReactOr) (up). Several techniques can be used, including magnetron sputtering, PECVD, reactive ion etching (RIE) or ion beam etching (IBE). PEDRO picture of Universitat de Barcelona (down).

The gas precursor has an important effect on the film's properties. Benzene (C_6H_6), for example, due to its low ionization potential provides a high growth rate but due to the high number of C atoms per molecule, a high bias voltage is required to get the desired 100 eV per ion. Acetylene (C_2H_2) ions, on the other hand, achieve already higher energies than C_6H_6 at similar bias voltages, 200 V. Acetylene and methane (CH_4) are the most popular choices to deposit DLC [16]. The latter has higher ionization potential and therefore lower growth rate, but opposed to acetylene it is available in high purity form. Methane also provides more hydrogenated films [11].

In this work, amorphous carbon (a-C) thin films have been deposited using PECVD technology powered with bipolar pulsed DC. RF excitation provides rather inefficient ionization in the plasma, with plasma densities about 10^9 cm^{-3} [1]. On the other hand, bipolar pulsed-DC does not have such limitation associated to RF excitation, so that big parts can be coated efficiently, using this technology. Regarding ion energy, the increased peak voltage for equal average power could provide more energetic ions than using RF at the same pressure [2].

Pulsed-DC deposition of DLC at medium frequency (50-350 kHz) presents some advantages over the more extended RF technique [Andújar et al., 2003]. On the other hand, this technique has shown an increase in deposition rate and a reduction of intrinsic stress, the latter being due to the changing polarity (bipolar characteristic) of cathode bias. This characteristic of the signal enables stabilization of the film during the positive period of each cycle, while for RF this voltage (self-bias DC) is always negative. In addition, with respect to RF, pulsed-DC also has the advantage of providing more energetic ions to the cathode. Although for equal power, mean cathode voltage is roughly the same for both signals, peak voltage is substantially higher for pulsed-DC than for RF.

B. Deposition conditions

The PECVD processes were carried out in a computer-controlled plasma reactor called PEDRO (Plasma Etching and Deposition ReactOr) of the FEMAN Group. It was built by Miguel Rubio Roy as a part of his PhD in the University of Barcelona (Fig. 1). Apart from the PECVD, other techniques are available: Magnetron Sputtering, Reactive Ion Etching (RIE) and an Ion Beam Etching (IBE). PEDRO has a main vacuum chamber of 80 litres of volume approximately and three load-lock chambers with their respective cathodes. The whole system is about 2 meters height per 2 meters long. The reactor is pumped down by means of a turbomolecular pump and the load-lock chambers are evacuated by rough pumping (low vacuum). With this system we could achieve a base pressure of 10^{-5} - 10^{-6} Pa. The cathodes can be connected to a high power supply to drive the voltage needed to switch on the plasma. Gas valves, pressure gauges and mass flow controllers are operated with a LabView interface, which also permits to run new and recorded depositions automatically. This software was performed by Miguel Rubio Roy.

Methane (CH_4) was used as a main carbon precursor. However, it is very difficult to deposit carbon on silicon because of adhesion problems on the substrate. Thus, the deposition process should take place with other important gas, CHF_3 , to improve surface properties of the layer. That is it, with the appropriate combination between gases containing carbon and fluorine we will first coat a substrate with carbon, where fluorinated-carbon films will be able to grow in a proper way. The chosen gases are methane (CH_4) and trifluoromethane (CHF_3). The idea is growing first a thin layer of hydrogenated carbon (a-C:H) on silicon surface, and finally, a film of hydrogen-fluorinated amorphous carbon (a-C:H:F).

The deposition of the films has been done at 10 Pa in power regulation mode at 57 W, which provided a negative peak voltage near to 1000 V, which represents an approximate power of 1.3 W/cm^2 . Moreover, pulse frequency and duty cycle were fixed to 100 kHz and 80%, respectively. These conditions had previously been observed to produce DLC films with average characteristics [2]. The CHF_3 relative flow has been set to 50, 75, 85 and 90% versus CH_4 , to study the

effects of the progressive fluorination of the films. The optimal gas combination was used to coat the nanostructured surfaces. The total gas flow was 25 sccm. PEDRO controller was able to deposit layers varying the concentration of the precursor gases in a gradient way until it gets the desired relative gas flow.

With a vacuum of 10^{-5} Pa prior to deposition, process took place with four phases: 1) start: only methane without discharge (120 s), 2) buffer layer: methane plasma (60 s), 3) gradient interface: gradient between CH_4 and CHF_3 with plasma (60 s); 4) stabilized proportion of gases with plasma (60 s). A total time process of 5 minutes was set, previously calculated to obtain a thin film of approximately 100 nm. Substrate was kept at room temperature by means of a water-cooling circuit, in order to grow amorphous films.

C. Lithography technique

Surface patterning has been performed by means of laser lithography using a Mask Plotter, DWL66 model Heidelberg Instruments, property of the Parc Científic of Barcelona. Mask Plotter can fabricate high resolution masks for photolithography to directly pattern substrates; lateral resolution goes down to 0.5 μm . This technique is advantageous to pattern sub-micrometric structures in a very large area in shorter time than using e-beam lithography.



Fig. 2. Mask Plotter of Parc Científic de Barcelona.

At present, using cell culture it is possible to produce a cellular growth, for example of fibroblasts or osteoblasts attached to a surface by means of a thin film of polylysine. In this work we intend to produce an adequate nanostructured substrate for biological/biomedical applications. DLC is a suitable candidate due to its bio-properties (anti-thrombosis, biocompatibility, chemical inertness) for building interfaces between a non biological substrate (surface lithographed c-Si) and the cell culture medium.

In this earlier phase we intend to produce suitable substrates for controlling experiments of self-assembly of inorganic nanoparticles. So, in this work we propose some particular structures consisting in tracks 2 μm wide but with different separation among themselves: 0.5, 1, 2 and 3 μm (Table I). Designed with the program CleWin 4, we patterned areas of about 4 cm^2 in approximately 120 minutes. Moreover these areas provided enough space to do all the characterization.

D. Characterization

After the deposition process we need to study the surface properties of the carbon films to test their efficiency. One of the first steps is measuring the thickness of the film. With a few pen marks before the deposition and removing it afterwards we can create a step to measure the thickness of the carbon film. Profilometry was carried out with a Dektak 3030. A stylus scans the surface and it measures with a nanometric precision in depth. We are interested in 100 nm thick films.

Wettability, which plays an important role in surfaces addressed to biomedical applications, has been characterized with a contact angle meter CAM 200 from KSV. This instrument is equipped with a multidispenser system that provided drops of deionised water. Pictures were captured with a camera either in static or in advancing (dynamic) mode.

Another important question is the friction and hardness of the layer. In this occasion we will use a nanotribometer from CSM with a home-made PID humidity controller, which will measure friction coefficient. It consists in a sliding WC ball (3 mm diameter) that scratches the surface in linear reciprocating mode. The applied load, 100 mN, was low enough to perform scans without damaging significantly the surface pattern.

A first approach to characterize the surface topography consisted in optical microscopy study of the samples. For this, we used an Olympus optical microscope with a 10X ocular and many objectives: 5, 10, 20 and 50X. We also used an Optical Imaging Profiler PL μ 2300 from Sensofar in interferometric and confocal modes, in order to increase image resolution. High resolution scanning electron microscopy (HR-SEM) observations were also needed in order to characterize the morphology of the lithographed structures and their final view with the attached SiO_2 nanoparticles. One of the microscopes used was a Strata DB235 from FEI Company, in Parc Científic de Barcelona, a field emission microscope with filament. The high-resolution mode can resolve 2-5 nm depending on the magnification: 50k, 100k, 200k, etc. The other SEM, in the Serveis Científic-Tècnics (SCT), is a Hitachi FE S-4100 scanning electron microscope.



Fig. 3. HR-SEM of Parc Científic, Barcelona

Finally, due to the limited height resolution of SEM, we used Atomic Force Microscope (AFM) Park XE-70 in non-contact mode to measure surface topography, in the Universitat de Barcelona. We also used an AFM Multimode

from Veeco in the *Serveis Científico-Tècnics, UB* (SCT-UB) operated in contact mode. The real heights of the lithographed tracks are needed to compare them after they are coated with the fluorinated carbon film.

E. Silica nanoparticles

The synthesis of spherical silica particles (SiO_2) was carried out by sol-gel method with a precursor of tetraethylorthosilicate (TEOS, high purity $\geq 99.0\%$, Fluka). Hydrolysis and condensation reactions were initiated by the addition of water diluted in ethanol. A small concentration of ammonia (NH_4OH , 25%, Merck) in the solution fixed the pH to basic. After stirring for a short time, the solution turned white which is the sign that the size of particles or their aggregates achieve the wavelength of visible light. After 1 h, the particles had reached their final size. Finally the residual chemicals were eliminated by centrifugation before collection of the sol-gel sub-micron particles and redispersion in fresh ethanol. The solution contained particles showing a very narrow size distribution (monodisperse) with an average size of 400nm [17].

III. RESULTS AND DISCUSSION

A. Lithographed structures

After the laser lithography developed by mask plotter we finally obtained four samples. The results of the lithographed structures on silicon are discussed below.

TABLE I
LITHOGRAPHED SAMPLES

Sample	Width (μm)	Separation (μm)
#1 (10G2701)	2	0.5
I (10G2704)	2	1
D (10G2703)	2	2
SP (10G2702)	2	3

Fig 4 shows the lithography of sample #1 after chemical etching of silicon, with no deposition and about 400 nm depth.

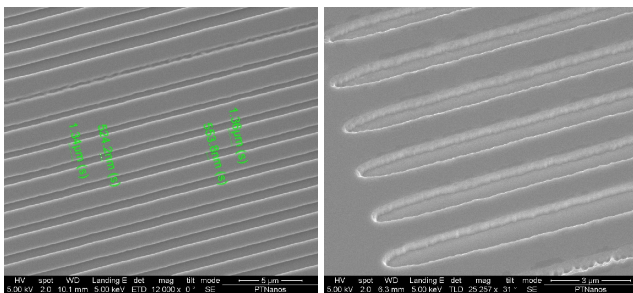


Fig 4. HR-SEM images of lithographed silicon of the sample #1 (2 μm wide and 0.5 μm of separation).

B. Deposition Conditions

The physical properties of the carbon layers depend directly on the deposition parameters [1]. Before depositing the a-C:H:F films on the lithographed silicon, we optimized the relative quantity of CHF_3 versus the CH_4 in depositions on flat

silicon wafers. The parameters to be optimized are contact angle and friction coefficient. After we made four tests with different concentration we did the respective tests in the contact angle and nanotribometer. We want the highest angle contact (hydrophobicity) and the lowest friction coefficient. The deposition process with a 90% of CHF_3 and 10% of CH_4 provided the sample showing the best compromise of tribological and surface properties (see table II). We did not go explore CHF_3 relative flows higher than 90% because friction coefficient increases dramatically beyond this point [1].

TABLE II
IMPROVING DEPOSITION CONDITIONS

Relative quantity of CHF_3 (sample)	Contact Angle ($^\circ$)	Friction Coefficient
50% (10G1901)	76.7	0.20
75% (10G2201)	76.7	0.20-0.21
85% (10G2302)	77.4	0.20-0.21
90% (10G2601)	78.9	0.23-0.24

So from now until the end of the paper, all the samples are coated with 90% of CHF_3 conditions. Total deposition time was 5 minutes long in order to obtain a thin film layer of about 100 nm thick. Thin enough to preserve/reproduce the topography of the substrate, and thick enough for their protective performance.

C. AFM

AFM images were obtained before and after the fluorinated carbon deposition on the lithography samples. The scan areas were 5x5 and 10x10 μm^2 . The goal is checking the height of the steps because the deposit of fluorine-carbon degrades in some way the topography of the substrate.

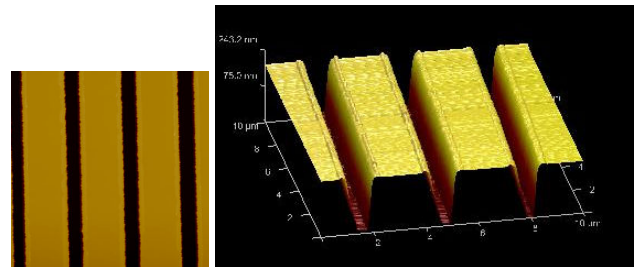


Fig 5. AFM images of the lithographed surfaces before the carbon deposition (left) and after (right).

In both cases the depth of the lithography is approximately the same, around 400 nm. We also can see that the deposition process keeps the shape of the lithography. So we can say that is a conformal process.

D. Contact Angle

In the static mode, it means that the needle drops individual droplets with a fixed volume. We used 2 or 3 water drops of about 5 μl each, so we will have a final drop of 10-15 μl of water. We did all the experiments at room temperature, around 25°C and a relative humidity of 50%. In the beginning, all the experiments contained in Table III correspond to the *static mode*. We chose 3 parts of every sample and we did a measure in them (Fig 7); after that, final values shown on the table were calculated through an arithmetic mean.

TABLE III
CONTACT ANGLE

Sample	Direction	Contact Angle (°)
10G2701 (0.5 μm and without carbon film)	orthogonal	37.5
	parallel	63.7
10G2701 (0.5 μm)	orthogonal	68.6
	parallel	110.0
10G2204 (1 μm)	orthogonal	75.8
	parallel	92.7
10G2603 (2 μm)	orthogonal	74.1
	parallel	97.9
10G2602 (3 μm)	orthogonal	76.6
	parallel	86.4

As we see in Fig 6 and Table III the difference in the contact angle of the droplet between the two directions (parallel and orthogonal) is significant, there is a big anisotropy (Fig 8). That is completely due to the lithography and it modifies the shape of the droplet. We can consider that the drop is on a group of pillars (Fig 6). The left and the right edges of the drop are constrained to move on the first and the last horizontal pillars, respectively. The equilibrium shape thus obtained is the local minimum of the free energy. The resultant equilibrium shape satisfies the condition that the mean curvature of the surface is constant. The local contact angle along the actual solid-liquid-fluid contact line is equal to the intrinsic contact angle [4]. The angle contact also increases substantially after the deposition process. That means that fluorinated carbon films are quite hydrophobic, i.e. repel water.

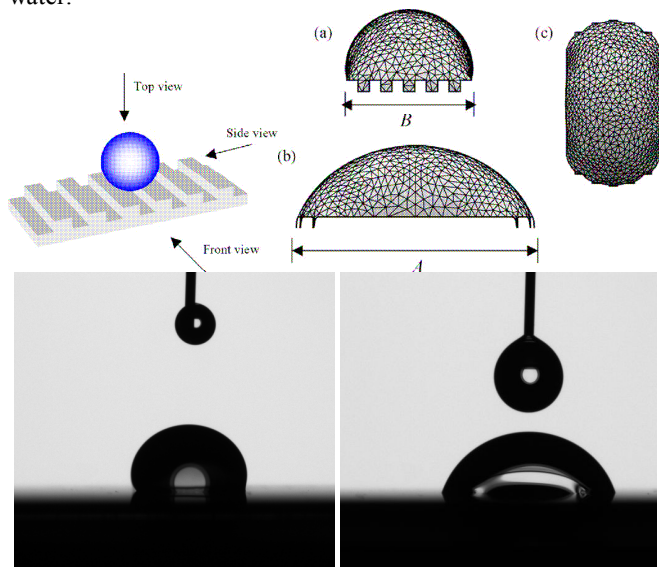


Fig 6. Up-Left. Drop on the pillars (lithography). Up-Right. a) Front view, b) Side view, c) Top view. [4] Down. Droplet of water when watching the droplet parallel to the lithography (front), and watching it orthogonal (side).

Another interesting experiment is the *advancing mode*. In this case, the needle is really close to the surface of the sample and it drops water with a continuous flow. In this configuration we can observe that contact angle increases dramatically with respect to static mode operation. We achieve contact angles very close to 180°, which means super hydrophobicity.

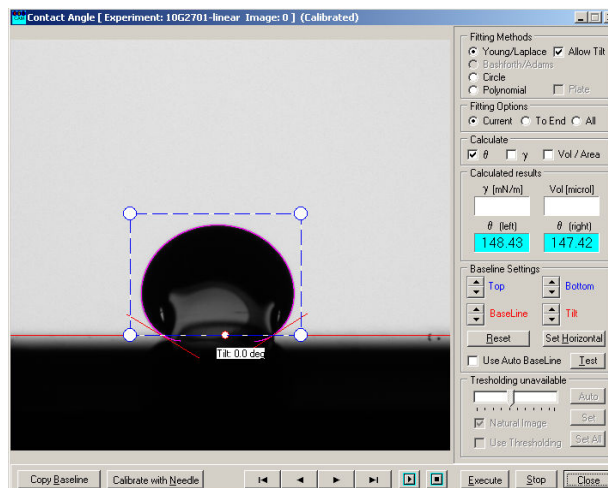


Fig 7. KSV program fitting a droplet in advancing mode

We also observed the dependence of the contact angle with the separation between the tracks. It seems that the contact angle values tend to be the ones with the flat surface when the distance of the tracks increases.

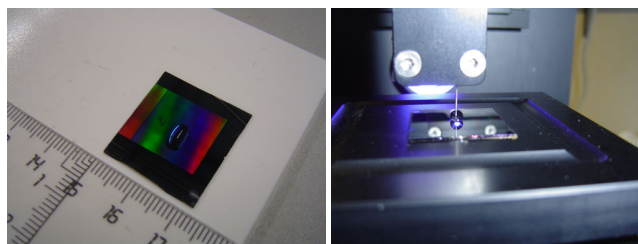


Fig 8. Images of the drop shape and the sample

E. Nanotribometer

Nanotribometer studies were the longest ones. Every sample takes an average of 2 hours in every direction, parallel and orthogonal to the lithography, with a mean velocity of 1 mm/s. The experiments were done at a room temperature of about 27°C and a constant relative humidity of 40%. The WC ball scratches the surface in linear reciprocating mode. Fig 9 shows a double line graphic, one line represents the scan forward, and the other line, the scan backward.

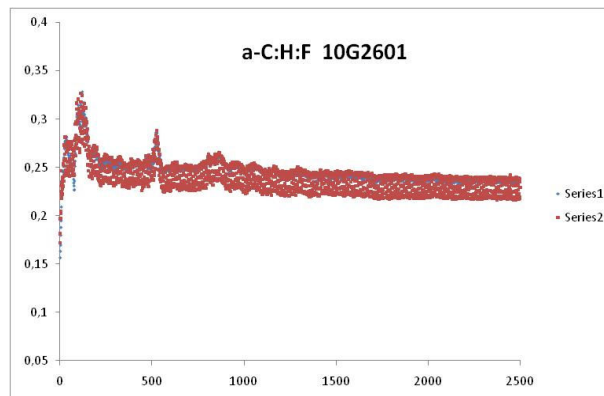


Fig 9. Graphic of the friction coefficient vs number of laps with the flat sample of silicon with a fluorinated carbon film (90% of CHF₃ conditions)

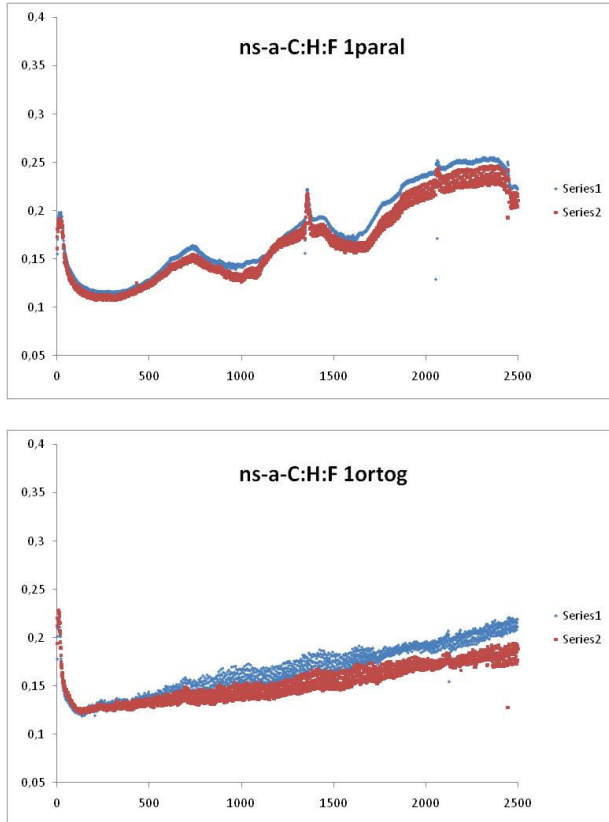


Fig 10. Friction coefficient vs number of laps with #1 sample (2 mm wide and $0.5 \mu\text{m}$ separation) in parallel (**up**) and orthogonal (**down**)

From Fig 10, we notice a lower friction coefficient with lithographed surface [14] and a different behaviour between parallel and orthogonal directions. While orthogonal tribology is more stable, parallel one is more irregular. A possible explanation could be that when the ball scratches parallel to the lithography, the debris produced by the ball remain in the channel and they affect the measurement. On the other hand, when the ball scratches orthogonally, the debris particles are more easily removed to both sides of the channel and through the valleys of the lithography. So, the channel is probably cleaner than in the other case and the measurement is more stable.

Fig 11 shows the path of the WC ball of the nanotribometer observed with an optical microscope. We can notice the differences between the parallel and orthogonal paths. The damage of the surface seems to be more important in the orthogonal one, but the amount of debris and wear particles is lower.

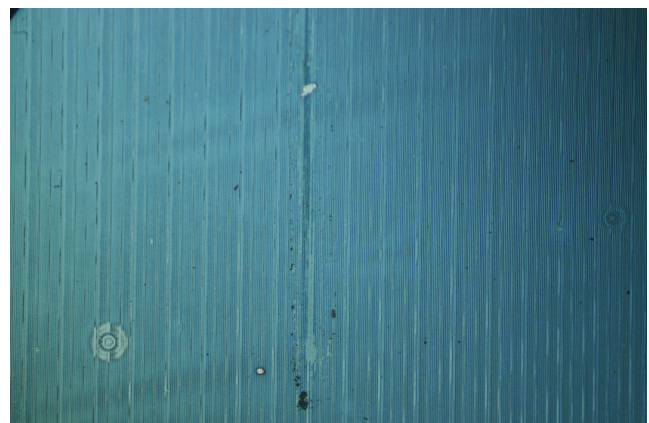
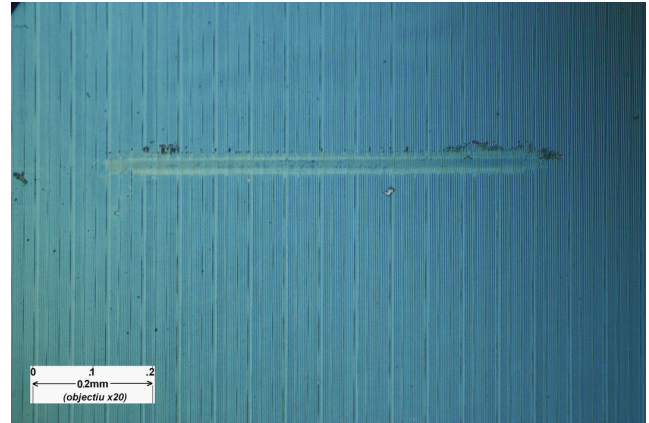


Fig 11. Optical microscope images with a 200X magnification, orthogonal (**up**) and parallel (**down**) to the lithography.

TABLE IV
FRICTION COEFFICIENT

Sample	Direction	Friction Coefficient
10G2701 ($0.5 \mu\text{m}$)	orthogonal	0.13
	parallel	0.12
10G2204 ($1 \mu\text{m}$)	orthogonal	0.27
	parallel	0.15
10G2603 ($2 \mu\text{m}$)	orthogonal	0.13
	parallel	0.21
10G2602 ($3 \mu\text{m}$)	orthogonal	0.21
	parallel	0.22

F. Silica nanoparticles and arrays

Silica nanoparticles were prepared with a monodisperse sol-gel solution during a whole day as explained above. The solution provides silica nanoparticles with a size around 400 nm, ideal for our purpose in the lithographed samples. The solution was dropped on the lithographed surface and it was homogeneously spread with two clean glasses orthogonally to the direction of the tracks. In this way, we obtained a monolayer of silica particles.

The optical imaging profiler provided the first results of the self-assembly of the silica nanoparticles. Fig 12 (up) shows clearly the pattern of the surface and the spherical silica particles attached to them. We also can see that bigger silica clusters do not fall into the valleys. Yellow beads correspond to the nanoparticles that are inside the pattern.

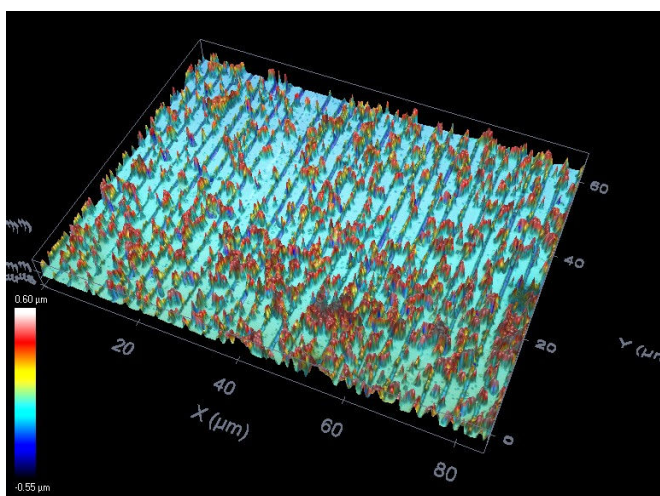
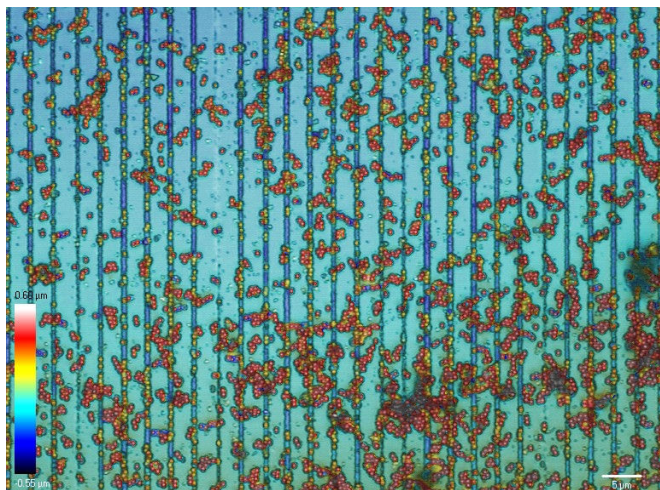


Fig 12. Confocal and interferometric images with 150X magnification, top view (up) and 3D (down).

The SEM of the SCT-UB has provided images with higher resolution. We can see in the figures Fig 12 and Fig 13 that the silica nanoparticles are visually aligned in arrays according to lithography. As we observe with more magnification (Fig 14 to Fig 16) we notice that most of the nanoparticles are really inside the valleys. The size of the particles is very homogeneous, around 500 nm, which helped us to identify the width of the valley. The number of particles inside is one (Fig 16) or two (Fig 14 and Fig 15) in width depending on the valley. Regarding to the depth of the valley, the number of particles is also one or at maximum two. So, the bigger the valley is, the more particles are deposited inside.

The alignment could be improved by increasing the width of the valleys of the lithography, the separation between tracks and spreading the particles more carefully.

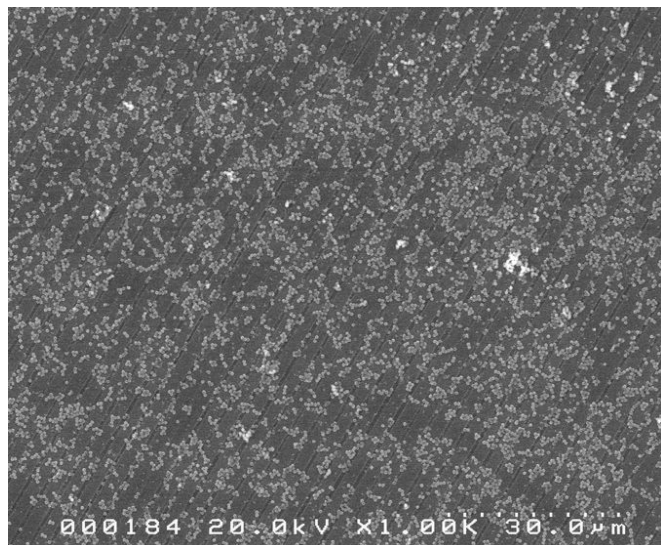


Fig 13. SEM image with 1000X magnification.

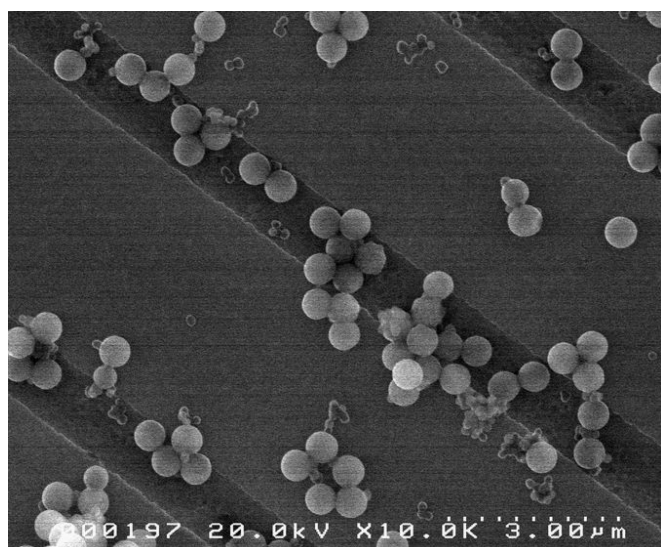


Fig 14. SEM image with 10000X magnification.

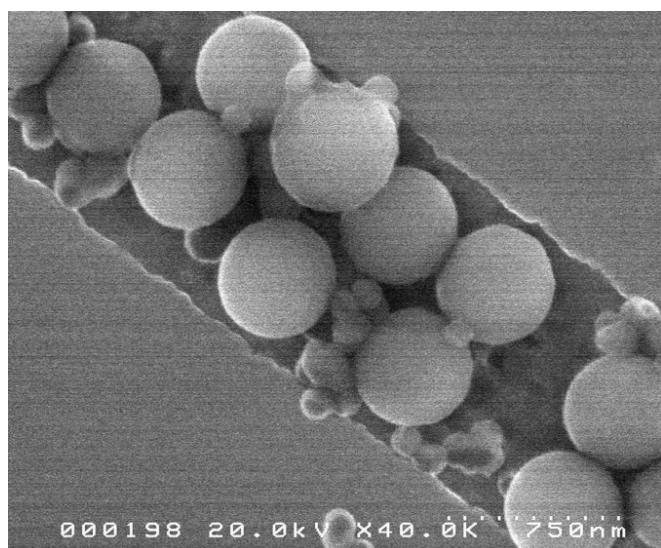


Fig 15. SEM image with 40000X magnification.

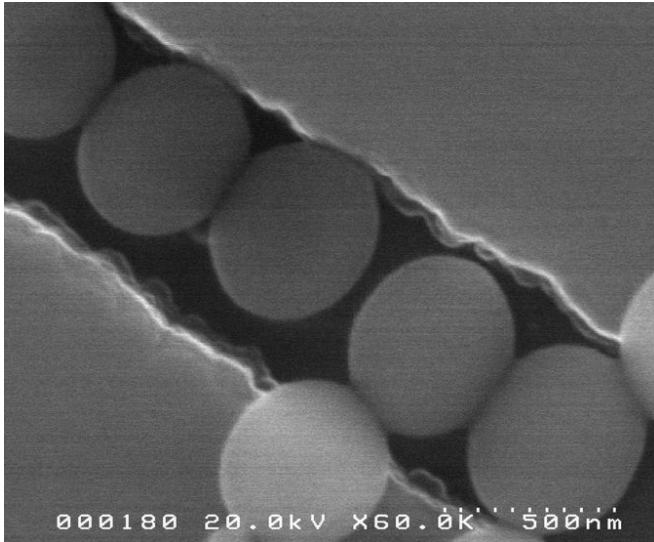


Fig 16. SEM image with 60000X magnification.

CONCLUSION

The best tribological (friction coefficient) and surface (contact angle) properties are met when performing the deposition process with the proportion of gases of 90% of CHF₃ versus 10% of CH₄ in relative gas flow.

Fluorinated-carbon films show hydrophobic character when operating in *static mode*, achieving super hydrophobicity in *advancing mode*.

There is a big anisotropy between parallel and orthogonal directions to the lithographed tracks. The presence of these patterns in the surface seems to increase the contact angle too.

In the tribologic studies, the first laps of the lithographed samples have a very low friction coefficient, just the opposite to the flat ones, which have an initial high peak. Moreover, there are differences between the orthogonal scan, quite homogeneous, and the parallel scan, more irregular. In average we notice a lower friction coefficient with lithographed surface.

Silica nanoparticles are arranged following the patterns successfully. It seems that the wider the valley is, the greater the possibilities to fall down are. So, bigger particles or clusters will find more difficulty to attach to the tracks than smaller ones, and the quantity of particles in it will also increase with big valleys than smaller ones. Although the width of the tracks are nominally identical, some tracks were accidentally wider and that is why we observed that effect.

ACKNOWLEDGMENT

The author thanks to FEMAN group, for letting him do his master thesis and research, for all the information shared and the nice moments. To Nasser, for the help with the Clean

Room of Universitat de Barcelona. To Parc Científic of Barcelona for its professional work and the kindness of David Izquierdo and Raúl Pérez. To Sabine Portal for her silica nanoparticles and self-assembly experiment. To Miguel Rubio for all his works and papers. To Carles Corbella, for all his knowledge and kindness, and Enric Bertran for showing me the world of scientific research.

REFERENCES

- [1] Miguel Rubio Roy, "Surface properties of Hard Fluorinated Amorphous Carbon Films Deposited by Pulsed DC discharges" PhD, Universitat de Barcelona, 2010.
- [2] Carles Corbella Roca, "Thin Film Structures of Diamond-like Carbon prepared by Pulsed Plasma Techniques" PhD, Universitat de Barcelona, 2005.
- [3] A. Grill, "Diamond-like Carbon coatings as biocompatible materials-an overview". *Diamond and Related Materials* 12 (2003) 166–170.
- [4] Yong Chen et al., "Anisotropy in the wetting of rough surfaces". *Journal of Colloid and Interface Science* 281 (2005) 458–464.
- [5] R. Hauert. "A review of modified DLC coatings for biological applications". *Diamond and Related Materials* 12 (2003) 583–589.
- [6] R. Hauert. "An overview on the tribological behavior of diamond-like carbon in technical and medical applications". *Tribology International* 37 (2004) 991–1003.
- [7] H. Kusumaatmaja et al., "Anisotropic drop morphologies on corrugated surfaces". *Langmuir* 24 (2008) 7299–7308.
- [8] Wen J. Ma et al., "DLC coatings: Effects of physical and chemical properties on biological response". *Biomaterials* 28 (2007) 1620–1628.
- [9] M Mastrangeli et al., "Self-assembly from mili- to nanoscale: methods and applications". *J. Micromech. Microeng.* 19 (2009) 083001.
- [10] S.C. Trippe et al., "Mechanical properties evaluation of fluor-doped diamond-like carbon coatings by nanoindentation". *Thin Solid Films* 446 (2004) 85–90.
- [11] J Robertson. "Diamond-like amorphous carbon". *Materials Science and Engineering R* 37 (2002) 129–281.
- [12] Ritwik Kumar Roy and Kwang-Ryeol Lee. "Biomedical Applications of Diamond-like Carbon Coatings: A review". Wiley InterScience (2007) DOI: 10.1002/jbm.b.30768.
- [13] R. Knizikevicius. "Simulation of silicon etching through a fluorocarbon layer". *Vacuum* 79 (2005) 119–123.
- [14] C. Corbella et al., "Surface structuring of diamond-like carbon films by colloidal lithography with silica sub-micron particles". *Diamond & Related Materials* 19 (2010) 1124–1130.
- [15] M. Grischke et al., "Variation of the wettability of DLC-coatings by network modification using silicon and oxygen". *Diamond and Related Materials* 7 (1998) 454–458.
- [16] S. Peter et al., "Comparative experimental analysis of the a-C:H deposition processes using CH₄ and C₂H₂ as precursors". *Journal of applied physics* 102 (2007) 053304.
- [17] S. Portal et al., "Influence of incident ion beam angle on dry etching of silica sub-micron particles deposited on Si substrates". *Thin Solid Films* 518 (2009) 1543–1548.
- [18] Seung-Man Young et al., "Nanomachining by Colloidal Lithography". *Small Journal* 2, No. 4 (2006) 458 – 475.
- [19] A. C. Ferrari, S. E. Rodil, J. Robertson, and W. I. Milne. "Is stress necessary to stabilise sp³ bonding in diamond-like carbon?" *Diamond and Related Materials*, 11(2002)994 – 999.